ADVANCED FUNCTIONAL MATERIALS

J. Andres, R. D. Hersch, J.-E. Moser and A.-S. Chauvin.
A New Anti-Counterfeiting Feature Relying on Invisible Luminescent Full Color Images Printed with Lanthanide-Based Inks,
in Advanced Functional Materials, vol. 24, num. 32, p. 5029-5036, 2014.

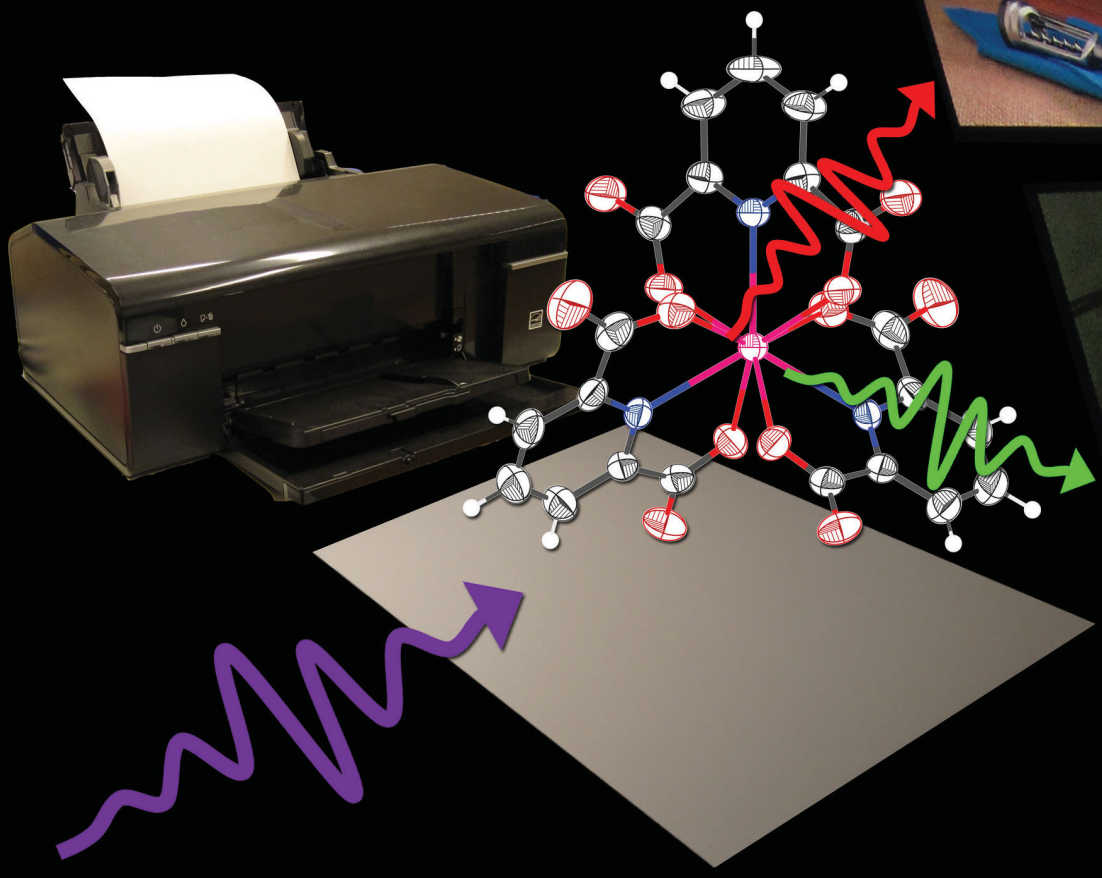

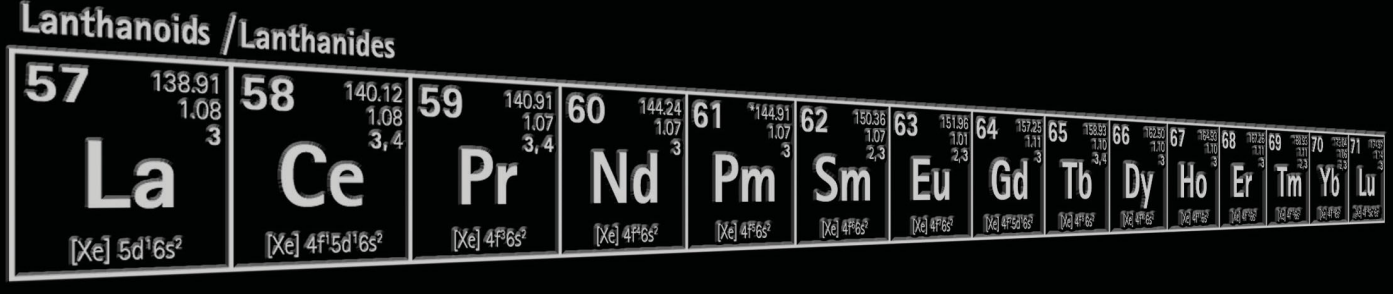

# A New Anti-Counterfeiting Feature Relying on Invisible Luminescent Full Color Images Printed with Lanthanide-Based Inks

*Julien Andres, Roger D. Hersch, Jacques-Edouard Moser, and Anne-Sophie Chauvin**

**Europium and terbium trisdipicolinate complexes are inkjet printed onto paper with commercially available desktop inkjet printers. Together with a commercial blue luminescent ink, the red-emitting luminescent ink containing europium and the green-emitting luminescent ink containing terbium are used to reproduce accurate full color images that are invisible under white light and appear under a 254 nm UV light. Such invisible luminescent images are attractive anti-counterfeiting security features. The luminescent prints have a color range (gamut) nearly as wide as the gamut of a standard sRGB display. The gamut of the luminescent prints is determined by relying on a simple model predicting the relative spectral radiant emittances of any printed luminescent color halftone. The model is also used to establish the correspondence between the surface coverages of the printed luminescent inks and the emitted color of these luminescent halftones. The accuracy of the spectral prediction model is very good and can be rationalized by the absence of quenching when the luminescent lanthanide complexes are printed in superposition with the other luminescent materials.**

## 1. Introduction

Counterfeiting is a growing global problem that challenges companies, governments and customers.[1] Anti-counterfeiting techniques that make genuine items harder to copy and easier to authenticate are therefore important for the protection of brands and valuable documents such as bank notes, diplomas and certificates. Luminescent tags or labels are appreciated security elements for protecting authenticatable articles. One way to incorporate luminescent materials as luminescent security elements is to print them with luminescent inks.[2] Nowadays, these printed luminescent security elements usually comprise only solid or halftone[3] single ink color patterns. Typical examples are bank notes that show luminescent parts under UV light (see Figure S3 in the Supporting Information, SI).

Procedures for producing full color images by printing luminescent inks exist.[4] These methods use several luminescent inks with different luminescent colors to form a full color image by luminescence. However, they are either colorimetrically inaccurate or use complex halftoning algorithms.

Many luminescent inks and markers, used for example as security inks, are made of lanthanide compounds.[5] The distinctive character of the emission from lanthanide ions, and particularly, their unique spectral fingerprints, enable the use of emissions and colors from lanthanide blends as security labels, markers or tags.[5d–5f]

Lanthanide ions are widely recognized for their exceptional luminescence. The forbidden nature of their *f-f* transitions and the shielding of the *f* electrons by more extended electronic shells enable achieving narrow spectral lines, which produce pure luminescent colors with long lifetimes.[6] Luminescent lanthanide ions are present in phosphors for lighting and display devices. Among the lanthanide series, europium and terbium ions are key elements for producing white light by combining red, green, and blue emissions (additive color synthesis).[7] Because of the low probability of their *f-f* transitions, the extinction coefficients of the lanthanide ions are very low, about a few L $mol^{-1}$ $cm^{-1}$. In order to efficiently harvest light and yield an important emission, luminescent lanthanide ions are usually photosensitized by organic chromophores with specific photophysical properties. These chromophores, sometimes called antennae, are embedded in ligands capable of coordinating trivalent lanthanide ions and forming complexes that are kinetically and thermodynamically stable.

Dipicolinic acid (dpa) is a tridentate ligand forming stable tris(dipicolinato) lanthanide complexes under stoichiometric

Dr. J. Andres, Dr. A.-S. Chauvin
École Polytechnique Fédérale de Lausanne
Faculté des Sciences de Base
Institut des Sciences et Ingénierie Chimiques
BCH 1405, CH-1015, Lausanne, Switzerland
E-mail: anne-sophie.chauvin@epfl.ch
Prof. R. D. Hersch
École Polytechnique Fédérale de Lausanne
Faculté Informatique et Communication
Laboratoire des Systèmes Périphériques
Station 14, CH-1015, Lausanne, Switzerland
Prof. J.-E. Moser
École Polytechnique Fédérale de Lausanne
Faculté des Sciences de Base
Institut des Sciences et Ingénierie Chimiques
Groupe de Dynamique Photochimique
Station 6, CH-1015, Lausanne, Switzerland



**DOI: 10.1002/adfm.201400298**

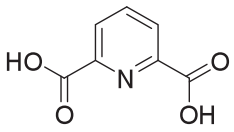


$pK_{a1}$ = 0.5
$pK_{a2}$ = 2.0
$pK_{a3}$ = 4.5

Eu:L
$\log\beta_{1:1}$ = 8.7
$\log\beta_{1:2}$ = 16.8
$\log\beta_{1:3}$ = 22.4

$H_2dpa$

$[Eu(dpa)_3]^{3-}$ $\Phi_L^{Eu}$ = 24 % $\tau_{obs}$ = 1.6 ms

$[Tb(dpa)_3]^{3-}$ $\Phi_{LTb}$ = 22 % $\tau_{obs}$ = 2.1 ms

**Scheme 1.** Dipicolinic acid: ligand structure, $pK_a$ values of the ligand stability constants of its europium and terbium complex with quantum yields and lifetimes in Tris-buffered solution (pH 7.4, 0.1 mM in complex). Values taken from the literature.[11,12]

conditions (hereafter trisdipicolinate complexes). The trisdipicolinate lanthanide complexes are water soluble and are stable in water at neutral pH, as shown by the log$\beta$ values displayed in **Scheme 1**. They also crystallize at high concentrations and were investigated by X-ray crystallography.[8] They display a tricapped trigonal prism structure typical of nine-coordinated ions. The tris structure is retained in aqueous solution at neutral pH, as proved, for example, by the lanthanide induced shifts,[9] and by the number of water molecules in the first coordination sphere obtained by measuring the observed lifetime in water and in deuterated water.[10] Europium and terbium trisdipicolinate have very attractive photophysical properties with high quantum yields and long lifetimes in the millisecond range (see Scheme 1).

Consequently, they are often used as standards for the determination of quantum yields.[11] Lanthanide trisdipicolinate complexes were also the main component of an aqueous inkjet ink composition in a patent application.[5c] However, they only absorb below 300 nm. The excitation of the ligand thus requires UV-C, which can be achieved by an uncoated mercury lamp with a UV bandpass filter. There are countless occurrences of dpa lanthanide complexes or complexes with dpa derivatives in the literature. Overviews of the different structures derived from dpa can be found elsewhere.[7a,13]

Color reproduction aims at reproducing original images on different media (e.g. prints, photographs, display devices, etc.) with the best possible color fidelity. In the case of prints, color reproduction aims at producing printed images with colors as close as the colors viewed on a display device.[14] In order to obtain a visually accurate and faithful reproduction of a color image on prints, a color reproduction workflow is used. This workflow consists of establishing the color domain (gamut) reproducible on the target prints, mapping original colors into printable colors,[15] and finding the correspondences between the desired mapped printed colors and the surface coverages of inks.

In this study, we propose to produce luminescent inks based on lanthanide complexes, printing them on paper with a desktop inkjet printer and forming thereby accurately reproduced invisible full color luminescent images. These full color images are visible only under UV light and can be used for anti-counterfeiting purposes. We used lanthanide trisdipicolinate complexes as luminescent dyes in the invisible luminescent inkjet inks and printed them with a commercially available inkjet printer. Since they do not absorb visible light, these inks are invisible. By exciting them with UV light, they become visible by luminescence. Full color luminescent images under UV light are reproduced by taking advantage of a specially conceived color reproduction workflow. The following luminescent inks are used: a red-emitting luminescent ink composed of europium trisdipicolinate, a green-emitting luminescent ink composed of terbium trisdipicolinate, and a commercially available blue-emitting luminescent ink. This commercial blue luminescent ink was selected because no blue-emitting dipicolinate complex providing a sufficiently high emission intensity was found. This selection of inks also allowed verifying that the luminescent lanthanide inks can be used together with an already existing commercial invisible luminescent ink. The ability of the luminescent lanthanide inks to be superposed with each other is tested first. Then, the three luminescent inks are used to reproduce full color images by luminescence. For that purpose, a model capable of predicting halftone emission spectra as a function of ink surface coverages has been established.

## 2. Results and Discussion

The red-emitting and green-emitting invisible luminescent inks were prepared from europium and terbium trisdipicolinate complexes respectively, as described in the experimental part given in SI. The ink formula prints properly (i.e. the ink is ejected from the printhead and forms visually well printed prints) both with a "bubble-jet" type Canon inkjet printer and with a "micro-piezo" type Epson inkjet printer (see SI for additional information about the printers). Two kinds of paper were used in this study: matte Canson paper and glossy Hahnemühle paper, both without fluorescent optical brightening agents. These papers were chosen for their outstanding quality, uniformity, and printability for inkjet. The procedure is yet also applicable to any non-fluorescent paper that is suitable for inkjet printing.

### 2.1. Effect of the Superposition of the Luminescent Inks

In order to test if the luminescent inks can be superposed with each other without quenching or disruption of the complexes, the inks were printed as solid (fulltone: 100% of surface coverage of the inks) luminescent samples. Time-resolved emission spectra of the lanthanide ions were measured under excitation with a pulsed nanosecond laser at 254 nm.

According to the observed lifetimes fitted from the emission decays, no quenching of the lanthanide ions occurs for the terbium complex, see **Figure 1**. The same behavior was observed with the europium complex. A luminescent ink can therefore be superposed with the other luminescent inks in prints without altering the photophysical properties of the lanthanide trisdipicolinate complexes.

The existing colorimetrically accurate color reproduction workflow developed by Hersch and coworkers was specially adapted to fluorescent inks that may induce quenching effects when the inks are on top of another.[4a] Since these luminescent inks are not quenching each other, a simpler procedure was developed.

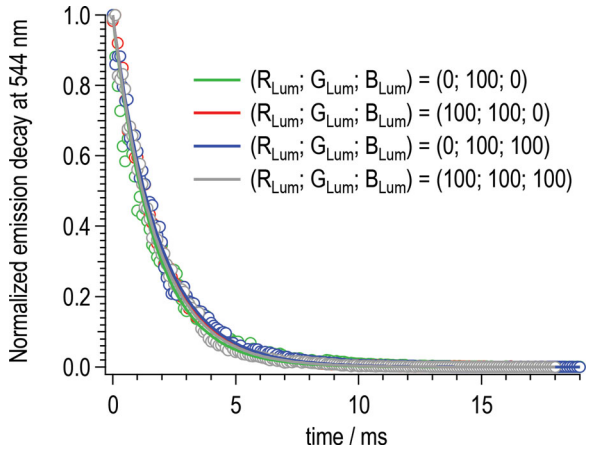


**Figure 1.** Normalized emission decay of the $^5D_4 \rightarrow {}^7F_5$ transition of $[Tb(dpa)_3]^{3-}$ for the green, yellow, cyan and white luminescent colorants.

### 2.2. Characterization of the Luminescent Halftones and Prediction of Their Emission

In order to confirm that the red-emitting, green-emitting and blue-emitting luminescent inks yield luminescent colors suitable for trichromic additive color synthesis, we printed them as luminescent halftones and measured their emissions under short wave UV light.

Excited by a 254 nm UV light source, the luminescent halftones were observed under a microscope. Their luminescent halftone structure is shown in **Figure 2**. Firstly, as seen in (B), the solid luminescent samples (surface coverage of 100%) do not entirely cover the surface. There is a regular line-like pattern that can also be observed on magnified solid samples printed with visible inks. This pattern is determined by the arrangement of the print-head nozzles and by other characteristics of the printer and its driver. Secondly, dot gain due to the lateral propagation of light within the substrate and to ink spreading (which is a well-known issue in color reproduction) can be observed in Figure 2. Compare the picture (D) of the luminescent color halftone with the ideal shaped luminescent dots shown in picture (E). Dot gain usually increases the effective dot surface coverages. These dot gain phenomena are further illustrated in SI (Figure S4) for the case of luminescent halftones. In order to account for dot gain, ink spreading curves are established which map nominal to effective ink dot surface coverages. This calibration step is performed by relying on a model predicting emission spectra as a function of ink surface coverages. The calibration samples comprise single ink halftones at 25%, 50%, and 75% surface coverages superposed with the bare paper, one ink and two inks.

The model for predicting the emission spectrum of any combination of luminescent ink surface coverages is based on the additive synthesis of emitted colors. As confirmed by Figure 2, the superposition of ink halftone dots yields additive colors. For the three luminescent inks, there are eight luminescent colorants that can be generated by superposition: red, green, blue, yellow (red + green), magenta (red + blue), cyan (green + blue), white (red + green + blue), and black (no luminescent ink). The surface coverages of these luminescent colorants define the

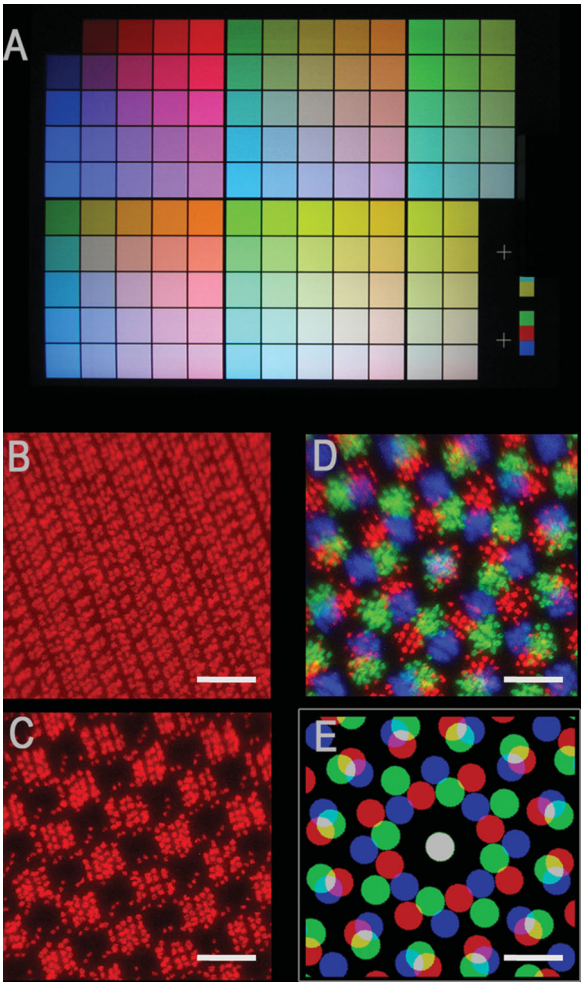


**Figure 2.** (A) Picture under UV light of the 125 luminescent samples printed on the Canson paper and printed by superposing the three luminescent inks at surface coverages from 0 % to 100% by steps of 25%; (B) Picture of the 100 % surface coverage of the red luminescent ink in A seen under a microscope; (C) Picture of the 50% surface coverage of the red luminescent ink in A seen under a microscope; (D) Picture of the luminescent color halftone at surface coverages (*r*, *g*, *b*) = (0.25, 0.25, 0.25) seen under a microscope; (E) Illustration of the ideally shaped luminescent dots of sample D. The thick white lines correspond to 1/100 of an inch (254 μm).

intensity of the resulting emittance relative to the emittance of the fulltone luminescent colorant. However, because of an inner filter effect on the luminescent inks (i.e., a decrease of the emission intensity due to the absorption of part of the UV excitation light source by superposed inks), the luminescent colorants produced by superposition of luminescent inks are not exactly the addition of the emission spectra of the superposed luminescent inks. Therefore, the different superpositions of the inks have to be taken into account when summing the emittances. This is done by defining the superpositions of inks as distinct luminescent colorants. **Figure 3** displays the emission spectra of all considered luminescent colorants, as well as the excitation spectra of the red, green and blue luminescent colorants. At the top of Figure 3, the base colorants are formed by the single luminescent inks printed as solid samples. In the

  

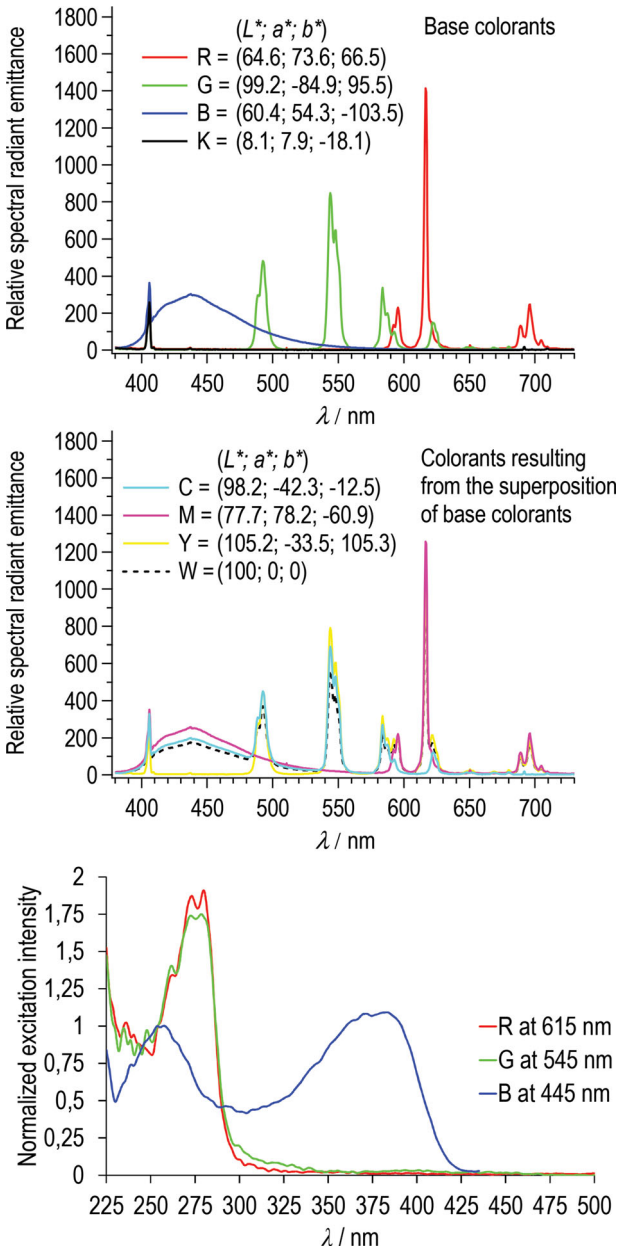


**Figure 3.** Top: Relative spectral radiant emittances, $E_f(\lambda)$ used in Equation (1) under excitation at $\lambda_{ex}$ = 254 nm, for the Canson Rag Photographique paper. The top graph shows the luminescent base colorants formed by the red emitting $Na_3[Eu(dpa)_3]$ 4.5%w ink solution, the green emitting $Na_3[Tb(dpa)_3]$ 5%w ink solution, the blue emitting commercial cyan Firefly ink and the unprinted paper black colorant. The graph in the middle shows the luminescent colorants obtained by superposing the R, G and B colorants. Bottom: Excitation spectra of the red, green and blue luminescent colorants (R, G, B) for their maximum emission at 615 nm, 545 nm and 445 nm respectively, normalized at 254 nm.

middle of Figure 3, the solid colorants resulting from the superposition of luminescent inks are shown. The bottom of Figure 3 shows the excitation spectra of the luminescent inks printed on Canson paper. These excitation spectra indicate that a UV light source at 254 nm (UV bandpass filtered uncoated mercury light) is suited for exciting all three luminescent inks, whereas

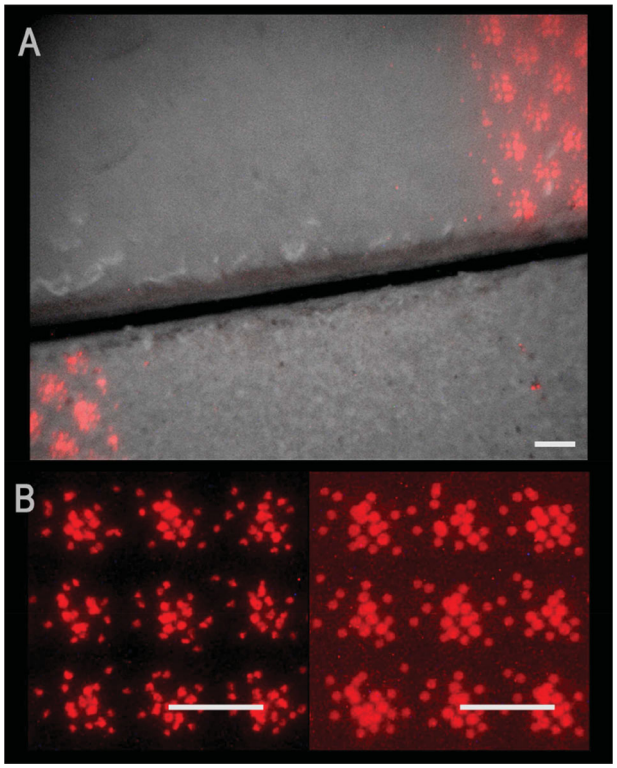


**Figure 4.** (A) Superposed picture of cut samples of the 25% surface coverage red luminescent halftone printed on the Canson paper (bottom, rough paper surface) and on the Hahnemühle paper (top, smooth paper surface) with the desaturated picture of the same sample observed under white light. (B) 3×3 cluster of screen elements showing different dot gains for the 25% surface coverage red luminescent halftone printed on the Canson paper (left) and on the Hahnemühle paper (right). The thick white lines correspond to 1/100 of an inch (254 μm).

a UV light source at 366 nm is only capable of exciting the blue luminescent ink.

Equation (1) predicts the emission spectrum (total relative spectral radiant emittance) of a luminescent halftone $E(\lambda)$, as the sum of the respective relative spectral radiant emittances $E_f(\lambda)$ of the eight luminescent solid colorants $f$, weighted by their surface coverages $a_f$. This spectral prediction model is similar to the spectral Neugebauer model used for predicting the reflectance spectra of color halftones.[16]

$$E(\lambda) = \sum_{f=1}^{8} a_f \cdot E_f(\lambda) \quad (1)$$

**Figure 4** shows the two studied papers viewed under a microscope and the impact the paper has on the luminescent halftones. On the matte rough surface of the Canson paper, the red luminescent halftone dots look more irregular than on the glossy smooth surface of the Hahnemühle paper. In addition, the glossy Hahnemühle paper seems to have more optical dot gain as seen by the red background compared to the much blacker one on the Canson paper. This observation is important since it indicates that luminescent halftones could be an efficient tool to investigate and characterize paper properties that are impossible to measure with normal color inks.

Besides the paper properties, dot gain also depends on the superposition of the inks. Therefore, a dot gain calibration needs to be established for each superposition condition. For three inks, the following cases are considered: each ink halftone alone, each ink halftone superposed with a second ink, and each ink halftone superposed with the two other inks. There are therefore twelve superposition conditions, which yield twelve dot gain curves.[17] Dot gain curves are obtained by subtracting the nominal surface coverages from the effective surface coverages. The effective surface coverages used to determine the dot gain curves are obtained by calibration, as reported in the experimental part (see SI). The resulting dot gain curves for each luminescent ink halftone superposed with paper, with one fulltone luminescent ink and with two fulltone luminescent inks are shown in SI (Figure S5). These dot gain curves depend on the paper and on the ink on which the halftone dot is superposed.

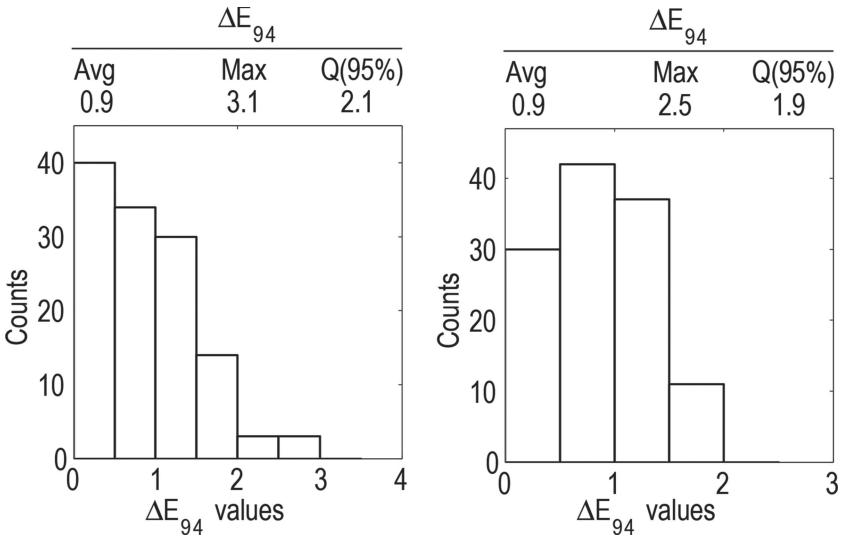


**Figure 5.** Distribution of the color differences between the measured and the corresponding predicted CIELAB colors on the Canson Rag Photographique paper (left) and on the Hahnemühle Photo Rag Baryta paper (right) with average (avg) maximum (max) and 95%-quantile values.

Once calibrated, the model was tested by comparing the predicted colors with the measured color on a set of samples representing the 125 combinations of 0%, 25%, 50%, 75% and 100% nominal surface coverages of the three inks (Figure 2A). This was done by measuring the relative spectral radiant emittances of the 125 luminescent samples, predicting the corresponding spectral radiant emittances according to Equation (1), converting the predicted and measured spectral radiant emittances to the CIE-XYZ color space and then to the CIELAB color space, and calculating the CIELAB $\Delta E_{94}$ color differences between the predicted and measured CIELAB colors. The reference white chosen for converting the CIE-XYZ tristimulus values to CIELAB colors was the luminescent white colorant formed by the superposition of the three inks. The CIELAB $\Delta E_{94}$ color differences between the measurements and the predictions give the accuracy of the prediction. The lower the $\Delta E_{94}$ color difference, the better the accuracy. Additional information about CIE-XYZ, CIELAB and the $\Delta E_{94}$ color difference can be found in the literature.[14] The equations used to calculate the colorimetrical values are presented in SI.

The detailed procedure for predicting emission spectra from nominal surface coverages of the luminescent inks is described in the experimental part (see SI). This procedure was applied to both papers. The $\Delta E_{94}$ color differences between the predicted and the measured colors were then calculated. For both papers, the distribution of the $\Delta E_{94}$ color differences between the emission predictions and the measurements for the 125 tested luminescent samples (see **Figure 5**) has an average $\Delta E_{94}$ value of 0.9 and a 95% quantile around 2.0. The maximal $\Delta E_{94}$ value is 3.1 on the Canson paper and 2.5 on the Hahnemühle paper. Since the average color difference between predicted and measured color samples is below 1.0 (visibility limit of the human visual system), the prediction accuracy of our model is excellent on both papers.

Such a good accuracy can be rationalized by the inertness of the lanthanide trispicolinate complexes when printed on top of each other or on the blue luminescent ink. The inner filter effect, which results in a lower emission intensity when superposing the inks, is not problematic since it is taken into account by measuring the emittances of the luminescent colorants (see Figure 3).

The prediction accuracy demonstrates that our ink formula yields halftones that are suitable for color reproduction. In addition, the good behavior of our custom inks proves that they are compatible with existing commercial inks and printers.

Since the model is accurate, the emission spectrum and hence the luminescent color of any luminescent halftone can be predicted precisely. The gamut of the colors spanned by the luminescent ink halftones can thus be determined from predicted luminescent colors. The spectral prediction model can also be used to find the surface coverages of the three luminescent inks that create a desired luminescent color under the UV bandpass filtered uncoated mercury light.

### 2.3. Visualization of the Color Range Offered by the Luminescent Inks

In order to determine the gamut (reproducible color range) of the luminescent ink halftones, the emittance of each combination of the surface coverages of the inks by steps of 2.5% of nominal surface coverage was first predicted, converted to CIE-XYZ tristimulus values, and then to CIELAB colors. The reference white is given by the emittance of the white luminescent colorant formed by the solid superposition (100 % surface coverages) of the three inks. From the resulting 68 921 CIELAB colors, the gamut boundary was computed by applying a Delaunay triangulation and then the ball-pivoting algorithm developed by Bernardini et al.[18] The spectral prediction model enabled us to calculate the 68 921 spectra instead of measuring them.

  

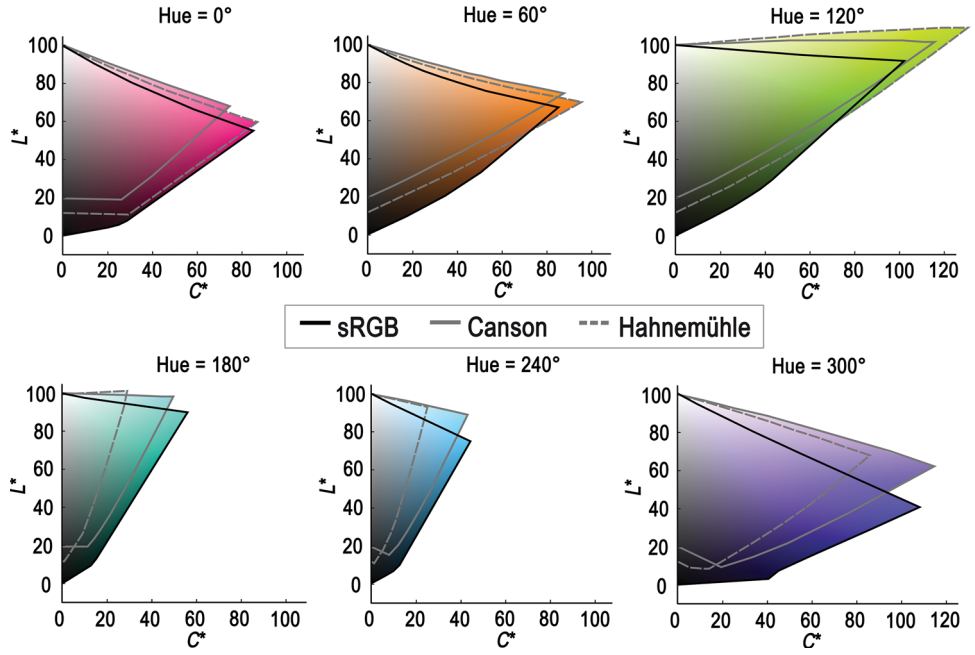


**Figure 6.** Gamut of the sRGB display colors and of the luminescent ink colors composed of $Na_3[Eu(dpa)_3]$, $Na_3[Tb(dpa)_3]$ and an unknown blue emitting compound printed on the Canson and on the Hahnemühle papers, displayed in the CIELAB color space.

As shown in **Figure 6**, the gamut of the luminescent ink halftones depends on the substrate on which they are printed. Furthermore, the white luminescent colorant used as the reference white color is different on the two papers. On the Canson paper, the white luminescent color looks more reddish than on the Hahnemühle paper. The white chromaticity is (x, y) = (0.31, 0.29) on Canson paper and (x, y) = (0.27, 0.28) on Hahnemühle paper. This may be explained by the following phenomena: the printed ink dots may penetrate and diffuse more or less in the paper, and the exciting UV light scatted by the paper may be subject to different inner filter effects depending on the ink superposition condition. Paper properties such as the coating, the glossiness, the scattering of the excitation UV light inside the paper, etc. may thus have an impact on the absorption of UV light by the individual inks and therefore induce different emissions of the ink dots forming the color halftones.

The colors of digital color images are generally defined in the sRGB color space that encloses the colors reproducible by standard sRGB display devices. Figure 6 shows both the gamut of a standard sRGB display and the gamut of the luminescent inks in the CIELAB color space. The gamut of the luminescent inks is close to the sRGB gamut in most hues, except in the blue colors where it is significantly smaller. Because of the inner filter effect that decreases the emission intensity of the colorants formed by superposed inks, the emission intensity of the white (superposition of the three inks) is lower than the emission intensity of the other colorants (Figure 3, right part). As a result, some colors with a green component have luminances higher than Y = 100, and hence, a lightness higher than $L^* = 100$. For the Canson paper, the yellow colorant has a lightness $L^* = 105.2$. For the Hahnemühle paper, the green ($L^* = 109.7$), yellow ($L^* = 108.9$) and cyan ($L^* = 101.3$) colorants have lightnesses higher than the lightness of the white. Therefore, at high lightnesses, the gamut in the green hues (with hue angles around $h_{ab} = 135°$) is larger than the corresponding sRGB gamut. This is also true, yet to a smaller extent, for the other hues.

Finally, the gamut of the luminescent inks does not include as many dark colors as the sRGB gamut. The lowest lightness on the greyscale axis achievable with the luminescent ink halftones is between 10 and 20. However, such dark colors are darker than the ones obtained in subtractive color synthesis by classical cyan, magenta and yellow inkjet inks. Let us also note that the unprinted paper does not look black, but bluish due to the reflection of a strong peak from the mercury lamp at 406 nm, despite the presence of a UV bandpass filter. This is confirmed by the fact that the lowest $L^*$ values are in the blue-violet hues.

### 2.4. Printing Invisible Pictures with the Luminescent Inks

Due to the large gamut of the luminescent inks, nice vivid images are expected with only little color differences between the input images viewed on an sRGB display and those observed under UV excitation. In order to print with the luminescent inks a faithful reproduction of a color image, the surface coverages of the luminescent inks enabling printing a given color are obtained by accessing a 3D lookup table that was constructed with the help of the spectral prediction model (detailed procedure in the experimental part). These surface coverages enable creating the red, green and blue luminescent ink separation layers. These separation layers are then halftoned according to the same method than the one used in the calibration of the spectral prediction model, i.e. with a classical rotated screen, having a round shape, at a screen frequency of


**Figure 7.** Photographs of a set of standard images reproduced with the luminescent inks on the Canson paper. On the left, a printed paper sheet under an A illuminant: the luminescent image is invisible. On the center, the same printed paper sheet under UV excitation at 254 nm: the luminescent images produced by the emission of the lanthanide complexes and of the blue emitting compound are visible and accurately reproduced. On the right, enlargements of the ski picture shown in the photograph on the center (i.e. viewed under UV light).

100 lpi, at orientations of 75° for the blue luminescent ink, 45° for the red luminescent ink and 15° for the green luminescent ink for the target printer resolution of 720 dpi. The halftoned luminescent ink layers are then printed on the corresponding paper with the Epson Stylus Photo P50 inkjet printer.

**Figure 7** displays a picture taken by a Canon PowerShot S95 digital camera of three standard images printed with the luminescent inks on the Canson paper. These three images represent a wide range of natural colors in the fruits, of saturated colors in the ski picture, and of people with skin tones in the orchestra image. They provide a good indication of the quality of the color reproduction. Additional photographs of the resulting luminescent images are presented as SI (Figures S6–S8).

## 3. Conclusions

For the first time, invisible full color luminescent images have been reproduced faithfully by printing luminescent inks containing lanthanide ions. The superposition of the europium and terbium trisdipicolinate inks enables reproducing colors from red to orange, yellow and green. The red emitting and green emitting luminescent inks were synthesized by diluting europium and terbium trisdipicolinate in a simple aqueous formula suitable for inkjet printing. In order to enable trichromatic additive color synthesis, the present lanthanide based red and green emitting inks are complemented by a commercial blue emitting luminescent ink.

The color reproduction workflow has been adapted to luminescent prints. The proposed simple spectral radiant emittance model predicting the emission of the printed luminescent halftones is accurate. This may be due i) to the stability and photophysical properties of the lanthanide complexes, and ii) to the fact that the color reproduction workflow comprises the measured emission spectra of the new colorants formed by the superpositions of the solid luminescent inks. The shadowing of the excitation light induced by the superpositions of the inks is thus taken into account.

The color gamut of the luminescent inks is wide and includes high chroma colors. At high lightnesses, it is larger than the sRGB gamut of a standard display device. The dark tones are not as dark as the ones of sRGB displays. However, they have a darkness similar to the one offered by classical inkjet printers. The images printed with the luminescent inks are pleasant and have a similar look as the images viewed on an sRGB display.

The potential of this application as anti-counterfeiting feature is attractive. Tagged documents can be easily authenticated by visualization under UV light. This document security feature cannot be counterfeited without the appropriate luminescent inks, and without the color reproduction software.

The color reproduction workflow and characterization procedure established in this work can be applied to other luminescent inks. Therefore, it provides a unique tool for the development of security features relying on luminescent prints.

In the future, we may consider the synthesis of a blue luminescent ink instead of the utilization of a commercial product. Complexes capable of sensitizing thulium and complexes with non-luminescent lanthanide ions have shown potential blue components in white light generation.[19] The sensitization of thulium has yet serious limitations.[20] We may thus turn towards blue ligand-centered emissions. Furthermore, the synthesis of new ligands capable of being excited at higher wavelengths may improve future luminescent dyes.

Regarding the cost of the luminescent inks, dipicolinic acid is commercially available and cheap (no need for a

  

time-consuming and expensive synthesis). It is therefore an excellent ligand because of its properties and availability. Lower purity lanthanide salts could also be used as long as no luminescent impurities change the emitted colors.

## Supporting Information

Supporting Information is available from the Wiley Online Library or from the author.

## Acknowledgements

The authors would like to thank Romain Rossier for his help and advice on colorimetry and for providing some of the matlab software modules further developed and used in this study. This study has been partly financed by the Swiss National Science Foundation, grants 200020_126757 and 200021_143501.

Received: January 27, 2014
Revised: March 12, 2014
Published online: May 22, 2014

[1] OECD, *The Economic Impact of Counterfeiting and Piracy*, OECD Publishing, Paris, Paris, **2008**.
[2] R. L. Van Renesse, *Optical Document Security*, Artech House, Boston **2004**.
[3] Halftoning converts continuous tone levels to ink dot surface coverages. When the size of the halftone dots is small, the halftone is perceived by a human viewer as a continuous tone. For more information, see C. Hains, S.-G. Wang, K. Knox, in *Digital Color Imaging Handbook* (Ed: G. Sharma), CRC Press, Boca Raton **2003**, pp. 385–490.
[4] a) R. D. Hersch, P. Donze, S. Chosson, Acm. T. Graphic, **2007**, article 75; b) W. J. Coyle, J. C. Smith, Angstrom Technologies, Inc., US Patent 7821675, 2010.
[5] a) J. D. Auslander, W. Berson, Pitney Bowes, US Patent 5542971, **1996**; b) B. A. Lent, G. G. Deng, J. F. Ezpeleta, The General Electric Company, Plc, WO 97/10307, **1997**; c) V. Aboutanos, T. Tiller, C. Reinhard, S. Rascagnères, SICPA Holding SA, US Patent 8,685,276, **2010**; d) G. A. Ross, P. Pollard, C. Hunter, S. Officer, G. R. Prabhu, NRC Corporation, US Patent, 7,129,506, **2004**; e) S. Officer, G. R. Prabhu, P. Pollard, C. Hunter, G. Ross, *Proc. SPIE-IS&T Electronic Imaging* **2004**, *5310*, 387–395; f) G. Kaur, Y. Dwived, A. Rai, S. B. Rai, *Spectrochim. Acta A: Mol. Biomol. Spectr.* **2012**, *95*, 511–516; g) Y. Liu, K. Ai, L. Lu, *Nanosc.* **2011**, *3*, 4804–4810; h) J. M. Meruga, W. M. Cross, P. S. May, Q. Luu, G. A. Crawford, J. J. Kellar, *Nanotech.* **2012**, *23*, 395201.
[6] J. Andres, A. S. Chauvin, in *The Rare Earth Elements: Fundamentals and Applications* (Ed: D. A. Atwood), John Wiley & Sons Ltd, Chichester, UK **2012**, pp.111–133.
[7] a) S. V. Eliseeva, J. C. G. Bunzli, *Chem. Soc. Rev.* **2010**, *39*, 189–227; b) S. V. Eliseeva, J. C. G. Bunzli, *New J. Chem.* **2011**, *35*, 1165–1176; c) L. D. Carlos, R. A. S. Ferreira, V. de Zea Bermudez, B. Julián-López, P. Escribano, *Chem. Soc. Rev.* **2011**, *40*, 536–549.
[8] a) L. VanMeervelt, K. Binnemans, K. VanHerck, C. GorllerWalrand, *B. Soc. Chim. Belg.* **1997**, *106*, 25–27; b) P. A. Brayshaw, J. M. Harrowfield, A. N. Sobolev, *Acta Crystallogr. C* **1995**, *51*, 1799–1802.
[9] a) C. N. Reilley, B. W. Good, *Anal. Chem.* **1975**, *47*, 2110–2116; b) H. Donato, R. B. Martin, *J. Am. Chem. Soc.* **1972**, *94*, 4129–4131.
[10] a) W. D. Horrocks, Jr., D. R. Sudnick, *Acc. Chem. Res.* **1981**, *14*, 384–392; b) A. Beeby, I. M. Clarkson, R. S. Dickins, S. Faulkner, D. Parker, L. Royle, A. S. de Sousa, J. A. G. Williams, M. Woods, *J. Chem. Soc., Perkin Trans.* **1999**, 493–503; c) M. Supkowski, W. D. Horrocks, *Inorg. Chim. Acta* **2002**, *340*, 44–48.
[11] A. S. Chauvin, F. Gumy, D. Imbert, J. C. G. Bunzli, *Spectrosc. Lett.* **2004**, *37*, 517–532.
[12] A. L. Gassner, C. Duhot, J. C. G. Bunzli, A. S. Chauvin, *Inorg. Chem.* **2008**, *47*, 7802–7812.
[13] a) K. Binnemans, *Chem. Rev.* **2009**, *109*, 4283–4374; b) J. Andres, A. S. Chauvin, in *The Rare Earth Elements: Fundamentals and Applications* (Ed: D. A. Atwood), John Wiley & Sons Ltd, Chichester, UK **2012**, pp.135–152.
[14] a) G. Sharma, in *Digital Color Imaging Handbook* (Ed: G. Sharma), CRC Press, Boca Raton **2003**, pp.1–114; b) H. G. Völz, in *Industrial Color Testing*, 2nd Ed., Wiley-VCH Verlag GmbH & Co. KGaA, Weinheim **2002**, pp.15–39.
[15] J. Morovic, in *Digital Color Imaging Handbook* (Ed: G. Sharma), CRC Press, Boca Raton **2003**, pp.639–685.
[16] J. A. S. Viggiano, *TAGA/ISCC Proc.* **1990**, 44–62.
[17] R. D. Hersch, F. Crete, *IS&T/SPIE Electronic Imaging Symposium, Color Imaging X* **2005**, *5667*, 434–447.
[18] F. Bernardini, J. Mittleman, H. Rushmeier, C. Silva, G. Taubin, *IEEE Trans. on Vis. and Comp. Graph.* **1999**, *5*, 349–359.
[19] B. W. Ennis, S. Muzzioli, B. L. Reid, D. M. D'Alessio, S. Stagni, D. H. Brown, M. I. Ogden, M. Massi, *Dalton Trans.* **2013**, *42*, 6894–6901.
[20] O. A. Blackburn, M. Tropiano, T. J. Sørensen, J. Thom, A. Beeby, L. M. Bushby, D. Parker, L. S. Natrajan, S. Faulkner, *Phys. Chem. Chem. Phys.* **2012**, *14*, 13378–13384.

ADVANCED FUNCTIONAL MATERIALS

# Supporting Information

for *Adv. Funct. Mater.,* DOI: 10.1002/adfm.201400298

# A New Anti-Counterfeiting Feature Relying on Invisible Luminescent Full Color Images Printed with Lanthanide-Based Inks

*Julien Andres, Roger D. Hersch, Jacques-Edouard Moser, and Anne-Sophie Chauvin**

Submitted to ADVANCED FUNCTIONAL MATERIALS



# Supporting Information

for *Adv. Funct. Mater.*, DOI: 10.1002/adfm.201400298

**A new anti-counterfeiting feature relying on invisible luminescent full color images printed with lanthanide-based inks.**

*Julien Andres, Roger D. Hersch, Jacques-Edouard Moser, Anne-Sophie Chauvin**

## Experimental part

Dipicolinic acid, europium(III) chloride hexahydrate 99.9 %, terbium(III) chloride hexahydrate 99.9 %, glycerol, ethylene glycol, diethylene glycol and isopropanol were ordered from Fluka and Aldrich and used without further purification.

*Formulation of luminescent inks*

The europium and terbium trisdipicolinate complexes were prepared and purified by crystallization as described elsewhere.[5c] The inks were prepared from these crystallized lanthanide complexes by dissolving them in a solution of distilled water (80 %w, weight percent), glycerol (7 %w), ethylene glycol (5 %w), diethylene glycol (5 %w) and isopropanol (3 %w). In this formula, water is the solvent, whereas ethylene glycol, diethylene glycol and isopropanol are co-solvents. Together with glycerol, ethylene glycol and diethylene glycol are also humectants, whereas isopropanol also acts as a defoamer. The europium trisdipicolinate red luminescent ink is produced by dissolving 4.5 %w of the crystallized europium complex in the ink solution at room temperature and filtering the resulting dyed solution through 0.45 μm filters. The terbium trisdipicolinate green luminescent ink is produced by the same procedure but contains 5 %w of the crystallized terbium complex dissolved in the ink solution.

The blue luminescent ink is a cyan Firefly™ ink manufactured by Vermont PhotoInkjet, LLC. The paper on which the luminescent inks were printed was either Canson Rag Photographique 210 g/m$^2$ sheets or Hahnemühle Photo Rag Baryta sheets.

*Luminescence measurements*

The time-resolved emission spectra used to fit the lifetimes were measured by exciting the printed luminescent samples with an Ekspla NT 342/3/UV pulsed laser. The excitation wavelength was set at 254 nm and gave a 6 ns pulse of 0.53 ± 0.04 cm$^2$ with a typical energy of 4 mJ at a frequency of 20 Hz. The resulting emissions were collected with an optical fiber and analyzed on a Hamamatsu photonic multichannel analyzer C8808 detector.

The emission spectra were measured with a MayaPro 2000 spectrophotometer from Ocean Optics. The captured emission spectra were corrected to account for the wavelength non-linearity of the detector and to yield relative radiometric units. The correction was performed using a calibrated DHL-2000-BAL lamp from Ocean Optics.

The excitation light source was a Camag laboratory UV lamp set at 254 nm. It consists in an 8 W uncoated mercury lamp filtered with a Schott UG11 UV bandpass filter glass. The lamp was placed at 30° relative to the normal direction of the surface of the samples. An optical fiber with a 600 μm diameter was used to collect light from the samples at 10° in the opposite direction.

The excitation spectra of the 100 % surface coverages of the luminescent inks (red, green and blue luminescent inks) printed on paper were measured with a Perkin Elmer LS50B spectrofluorimeter mounted with sample holder adapted for prints.

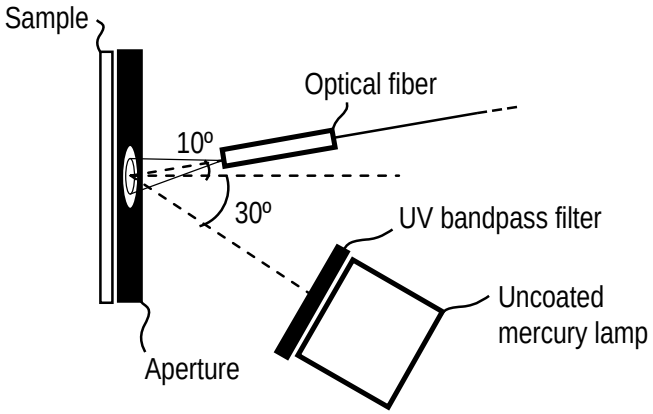


**Figure S1.** Setup used for measuring relative spectral radiant emittances of luminescent samples excited under 254 nm UV light

*Printing of the luminescent inks*

The luminescent inks were printed on two commercially available "desktop" inkjet printers. For the investigation of the effect of superposing the luminescent inks, a Canon Pixma iP4000 inkjet printer was used. For the color reproduction part of this study, an Epson Stylus Photo P50 inkjet printer was used. The Canon printer is a thermal inkjet printer (bubblejet technology) that heats the ink in order to expel it from its printhead. On the other hand, the Epson printer is a piezo inkjet printer (micropiezo technology) that mechanically pushes the ink out of its printhead. The printers were loaded with commercially available empty cartridges filled with the luminescent inks.

The printers were driven by custom drivers developed at the peripheral systems laboratory (LSP) of the École Polytechnique Fédérale de Lausanne (EPFL). These drivers enable full control of the printers, without any further color management or re-halftoning. This makes possible controlling the surface coverage of each ink individually.

The samples used for investigating the superposition of the luminescent inks were printed as solid samples (100 % surface coverages). The samples used for investigating the color reproduction ability of the luminescent inks were printed as halftones at combinations of 0 %, 25 %, 50 %, 75 % and 100 % surface coverages. The halftoning screen was round shaped

with a screen frequency of 100 lines per inch (lpi) and was printed at 720 dots per inch (dpi). The screen angle was 75° for the blue, 45° for the red and 15° for the green luminescent ink halftone layer.

*Color reproduction*

Color reproduction aims at reproducing original images on different media (e.g. prints, photographs, display devices, etc.) with the best possible color fidelity. For accurate color reproduction, the range of colors (gamut) of an original image has to be determined. Then the gamut of the target printer has to be found. Finally, one needs to map the gamut formed by all input colors into the gamut formed by all colors of the target printer, in the present case by the luminescent emissions of the ink hafltones.

In order to print the desired colors, one needs to establish a correspondence between colors and surface coverages of the luminescent inks. For this purpose, we rely on a spectral prediction model.

The main steps for producing luminescent full color images visible under UV were the following: First, the lightness range of input sRGB colors was linearly mapped into the lightness range of the output color gamut spanned by the luminescent inks. The second step consisted in mapping the lightness mapped sRGB CIELAB colors into the gamut of the luminescent inks according to a multiple foci gamut mapping algorithm (**Figure S2**, $L^*_{low} = 40$, $L^*_{high} = 80$).[1] Finally, the model predicting the relative spectral radiant emittances as a function of the surface coverages of the luminescent inks dots was used to obtain the surface coverages of the luminescent inks that reproduce the desired mapped CIELAB colors.

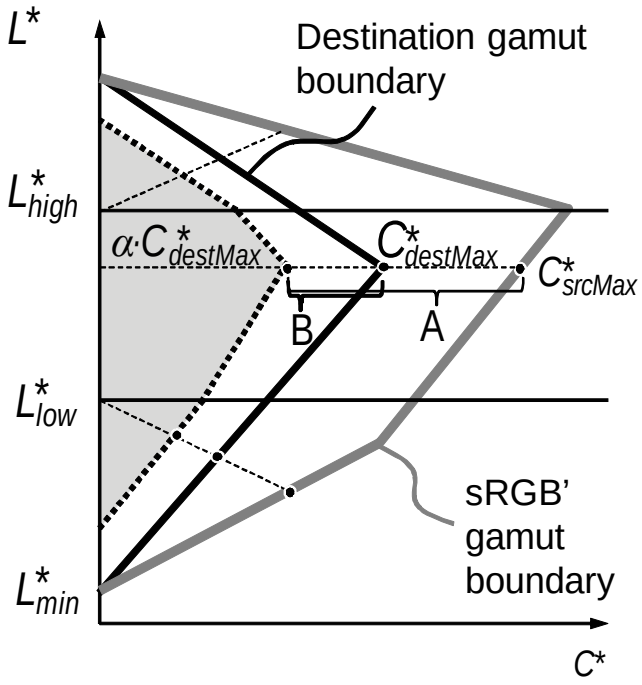


**Figure S2.** Multiple foci gamut mapping algorithm used to map the colors of the lightness mapped sRGB gamut into destination gamut. The intervals A are linearly mapped into intervals B. In the core area of the destination gamut (dark gray region determined by the $\alpha$ parameter), the colors remain the same.

To quickly establish the correspondences between the mapped CIELAB colors and the correct surface coverages of the luminescent inks, a 3D lookup table was created. This lookup table consists in a 3D grid in CIELAB with the precomputed corresponding surface coverages of the red emitting, green emitting and blue emitting luminescent ink at each CIELAB position of the grid (i.e., for each CIELAB colour in the grid). At image generation time, the desired mapped CIELAB colours present in the image are located in the 3D grid, and the corresponding surface coverages of the luminescent inks are interpolated from neighbour vertices.

*Calibration of the spectral prediction model*

The effective surface coverages were determined as follow. First, a set of calibration samples was measured. It encloses the eight solid colorants and the 25 %, 50 % and 75 % nominal surface coverages of each ink for each superposition condition (i.e., alone, on each solid individual ink, and on the solid colorants formed by the superposition of the two other inks). The effective surface coverages of each ink for each superposition condition were then fitted according to Equation (1) by minimizing the root mean square difference between the predicted emittances and the measured ones. This procedure yielded the twelve dot gain curves in **Figure S4**.

*Prediction of emission spectra by the spectral model*

For the prediction of the emission spectra, the effective surface coverages ($r'$, $g'$, $b'$) of the three luminescent inks for input nominal surface coverages are found according to the ink spreading equations (Equation S1). These equations are solved iteratively by starting with the nominal surface coverages ($r$, $g$, $b$). The ink spreading functions $f_{i/j}(u)$ represent the interpolated effective surface coverage of ink $i$ printed on solid colorant $j$ for an input nominal surface coverage $u$.

$$\begin{aligned} r' &= f_{r/k}(r)\cdot(1-g')\cdot(1-b') + f_{r/g}(r)\cdot g'\cdot(1-b') + f_{r/b}(r)\cdot(1-g')\cdot b' + f_{r/c}(r)\cdot g'\cdot b' \\ g' &= f_{g/k}(g)\cdot(1-r')\cdot(1-b') + f_{g/r}(g)\cdot r'\cdot(1-b') + f_{g/b}(g)\cdot(1-r')\cdot b' + f_{g/m}(g)\cdot r'\cdot b' \\ b' &= f_{b/k}(b)\cdot(1-r')\cdot(1-g') + f_{b/g}(b)\cdot g'\cdot(1-r') + f_{b/r}(b)\cdot(1-g')\cdot r' + f_{b/y}(b)\cdot r'\cdot g' \end{aligned} \quad \text{(S1)}$$

The surface coverages of the colorants $a_j$ are obtained from the effective surface coverages of the inks ($r'$, $g'$, $b'$) according to the Demichel equations (Equation S2). These equations calculate the surface coverages the colorants for the surface coverages $r'$ of the red, $g'$ of the green and $b'$ of the blue ink dots, when these dots are independently placed on the halftone surface.

$$
\begin{aligned}
a_k &= (1-r')\cdot(1-g')\cdot(1-b') & a_y &= r'\cdot g'\cdot(1-b') \\
a_r &= r'\cdot(1-g')\cdot(1-b') & a_m &= r'\cdot b'\cdot(1-g') \\
a_g &= g'\cdot(1-r')\cdot(1-b') & a_c &= g'\cdot b'\cdot(1-r') \\
a_b &= b'\cdot(1-r')\cdot(1-g') & a_w &= r'\cdot g'\cdot b'
\end{aligned}
\qquad \text{(S2)}
$$

The effective surface coverages of the luminescent colorants $a_f$ obtained with Equation S2 are then used in Equation (1) to weight the emission spectra of the luminescent colorants, $E_f(\lambda)$, and to predict the emission spectrum of the halftone printed with the ($r$, $g$, $b$) nominal surface coverages of the luminescent inks.

**Supplementary figures**


**Figure S3.** Fifty euro bank note shown under UV light and displaying luminescent parts (taken from Wikipedia)

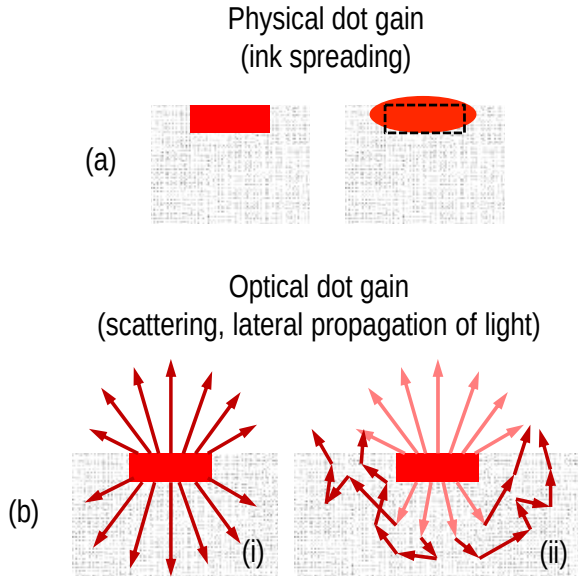


**Figure S4.** (a) Dot gain due to ink spreading and (b) dot gain due to lateral propagation of light emitted from the luminescent halftone dot. (i) No dot gain, (ii) "random walk" sattering of light in the paper bulk.

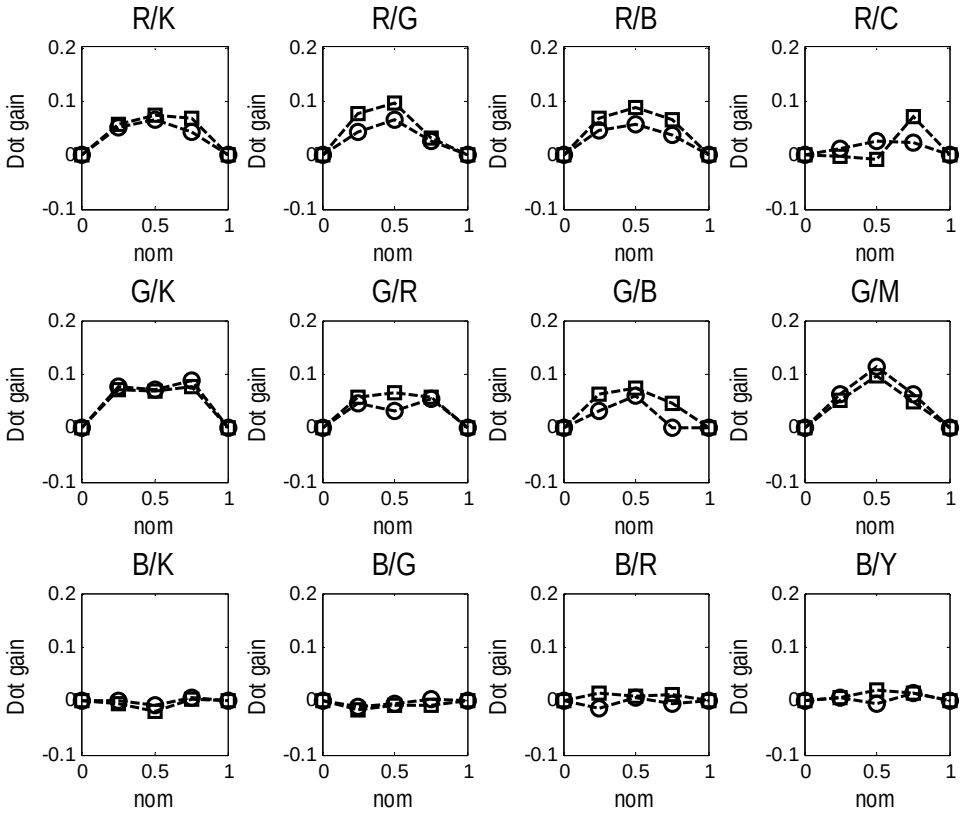


**Figure S4.** Dot gain curves for the red (R), green (G) and blue (B) luminescent halftones superposed on paper (K), with fulltone red (/R), fulltone green (/G), fulltone blue (/B), fulltone green and blue (/C), fulltone red and blue (/M) and fulltone green and red (/Y) on Canson Rag Photographique paper (circles) and on Hahnemühle Photo Rag Baryta paper (squares).

**Figure S5.** Photographs of the fruits, ski and orchestra luminescent images printed on the Canson paper (left) and on the Hahnemühle paper (right)

**Figure S6.** Photographs of luminescent images (the Balmoral Hotel in Edinburgh and the coast of the Isle of Skye in Scotland) printed on the Canson paper (left) and on the Hahnemühle paper (right)

**Figure S7.** Photographs of luminescent images (a sunset, a Ferrari and a black and white picture) printed on the Canson paper (left) and on the Hahnemühle paper (right)

**Colorimetric equations**

The XYZ tri-stimulus values were calculated according to (S3) from the relative irradiances $S(\lambda)$ and from the color matching functions $\bar{x}(\lambda)$, $\bar{y}(\lambda)$, and $\bar{z}(\lambda)$ of the CIE-XYZ color space. These functions are defined over $\lambda_{vis}$: the visible wavelength range from 380 nm to 730 nm. In our case, these functions were interpolated to match the resolution of the spectrometer (i.e. 0.5 nm steps).

A scaling factor K ensures that the brightest white stimulus $S_{ref}(\lambda)$ has a Y value of 100.

$$\begin{aligned} X &= K \cdot \int_{\lambda_{vis}} \bar{x}(\lambda) \cdot S(\lambda) \cdot d\lambda \\ Y &= K \cdot \int_{\lambda_{vis}} \bar{y}(\lambda) \cdot S(\lambda) \cdot d\lambda \\ Z &= K \cdot \int_{\lambda_{vis}} \bar{z}(\lambda) \cdot S(\lambda) \cdot d\lambda \\ K &= \frac{1}{\int_{\lambda_{vis}} \bar{y}(\lambda) \cdot S_{ref}(\lambda) \cdot d\lambda} \end{aligned} \qquad \text{(S3)}$$

The chromaticity coordinates xy were are obtained by dividing each tri-stimulus values by the sum of the tri-stimulus values (S4).

$$\begin{aligned} x &= \frac{X}{X+Y+Z} \\ y &= \frac{Y}{X+Y+Z} \\ z &= 1-x-y \end{aligned} \qquad \text{(S4)}$$

The CIELAB coordinates were calculated according to (S5) from the CIE-XYZ tri-stimulus values, providing a reference tri-stimulus value ($X_n$; $Y_n$; $Z_n$) that represents the white point of the color space, i.e. the ($L^*$; $a^*$; $b^*$) = (100; 0; 0) coordinate. Note that the scaling factor K

from (S3) should be the same in the calculation of the CIE-XYZ of the sample ($X$; $Y$; $Z$) and of the white reference ($X_n$; $Y_n$; $Z_n$).

$$
\begin{aligned}
L^* &= 116 \cdot f\left(\frac{Y}{Y_n}\right) - 16 \\
a^* &= 500 \cdot \left[ f\left(\frac{X}{X_n}\right) - f\left(\frac{Y}{Y_n}\right) \right] \\
b^* &= 200 \cdot \left[ f\left(\frac{Y}{Y_n}\right) - f\left(\frac{Z}{Z_n}\right) \right] \\
f(t) &= \begin{cases} t^{\frac{1}{3}} & \text{if } t > \left(\frac{6}{29}\right)^3 \\ \frac{1}{3} \cdot \left(\frac{29}{6}\right)^2 \cdot t + \frac{4}{29} & \text{otherwise} \end{cases}
\end{aligned}
\qquad \text{(S5)}
$$

The chroma or chrominance $C_{ab}^*$ and the hue $h_{ab}$ used for drawing the CIELAB color gamuts were calculated from the CIELAB colors according to (S6).

$$
\begin{aligned}
C_{ab}^* &= \sqrt{a^{*2} + b^{*2}} \\
h_{ab} &= \operatorname{atan} 2\left(\frac{b^*}{a^*}\right)
\end{aligned}
\qquad \text{(S6)}
$$

The $\Delta E^*_{94}$ color differences were calculated from the CIELAB colors according to (S7).

$$
\begin{aligned}
\Delta L^* &= L_1^* - L_2^* \\
\Delta a^* &= a_1^* - a_2^* \\
\Delta b^* &= b_1^* - b_2^* \\
\Delta E_{ab}^* &= \sqrt{\Delta L^{*2} + \Delta a^{*2} + \Delta b^{*2}} \\
\Delta C_{ab}^* &= C_1^* - C_2^* \\
\Delta H_{ab}^* &= \sqrt{\Delta E_{ab}^{*\,2} - \Delta L^{*2} - \Delta C_{ab}^{*\,2}} \\
\Delta E_{94}^* &= \sqrt{\Delta L^{*2} + \left(\frac{\Delta C_{ab}^*}{1 + 0.045 \cdot C_1^*}\right)^2 + \left(\frac{\Delta H_{ab}^*}{1 + 0.015 \cdot C_1^*}\right)^2}
\end{aligned}
\qquad \text{(S7)}
$$

**Supplementary references**

[1] J. Morovic, M. R. Luo, *J Imaging Sci Techn* **2001**, *45*, 283-290.